Catalysis Communications 158 (2021) 106335

Contents lists available at ScienceDirect

Catalysis Communications

journal homepage: www.elsevier.com/locate/catcom

Short communication

Spatially-resolved reaction profiles in Fischer-Tropsch synthesis – influence of operating conditions and promotion for iron-based catalysts

Florian Wolke [a,*], Yiwen Hu [a], Michael Schmidt [b], Oliver Korup [c], Raimund Horn [c], Erik Reichelt [a,*], Matthias Jahn [a], Alexander Michaelis [a]

[a] Fraunhofer Institute for Ceramic Technologies and Systems IKTS, Winterbergstraße 28, 01277 Dresden, Germany
[b] Reacnostics GmbH, Am Kaiserkai 30, 20457 Hamburg, Germany
[c] Hamburg University of Technology TUHH, Eißendorfer Straße 38, 21073 Hamburg, Germany

ARTICLE INFO

Keywords:
Fischer-Tropsch synthesis
Reaction profile
Iron catalyst
In-situ analysis

ABSTRACT

The complex reaction mechanism of iron-based Fischer-Tropsch synthesis comprises of manifold primary and secondary reaction pathways. Within this work, an experimental setup for spatially-resolved measurements on promoted iron-based Fischer-Tropsch catalysts is presented, allowing for a general study of the influence of operating conditions and promotion as well as of the influence of secondary reactions on product selectivity. It was found that, depending on catalyst composition, considerable hydrogenation of 1-alcohols and olefins occurs, while no considerable influence of reinitiation of chain growth on product distribution could be found.

1. Introduction

Conversion of syngas derived from renewables into valuable chemicals via Fischer-Tropsch (FT) synthesis represents a key process step of Power-to-X technologies allowing for the production of synthetic fuels and valuable chemical products [1,2]. Due to its eco-friendliness, low price level and versatility, iron is recognized as a suitable material for FT catalysts and a considerable number of respective studies was published over the last decades [3,4]. The FT reaction is well-known for its multifaceted polymerization mechanism. Even though the first studies of Fischer and Tropsch can be dated back to the 1920s, the underlying mechanism as well as the active catalyst phases – especially in iron-based FT synthesis – are not completely understood so far [5–8]. In detail, FT mechanism comprises a high number of main and side reactions, which are affected by reaction kinetics and transport characteristics [9,10]. There is a consensus in literature that Fischer-Tropsch synthesis cannot be described by a single mechanism. Among the proposed mechanisms, the carbide mechanism – allowing to explain the formation of paraffins and olefins – and the CO insertion mechanism – also allowing to describe the formation of oxygenates – are most frequently discussed [8,11].

Several efforts regarding deeper insights into the complex FT reaction were made. Especially, in order to elucidate the structure-activity and structure-selectivity relationships, in-situ analytics were applied [12]. To measure the catalyst phase composition, experimental setups for structural analysis, e.g. in-situ X-ray diffraction spectroscopy (XRD) or in-situ Mössbauer spectroscopy (MES) were developed and applied [13,14]. Additionally, methods based on absorption of X-ray radiation, e.g. in-situ X-ray absorption fine structure measurements (XAFS) or in-situ wide angle X-ray scattering analyses (WAXS) were presented [15]. Another applied approach were microscopic methods, e.g. in-situ environmental transmission microscopy combined with electron energy loss spectroscopy (ETEM-EELS) [16].

However, these methods are only addressing the in-situ observation of changes in the catalyst structure. Additionally, in many of the mentioned in-situ setups, the applied reaction conditions are far from the industrial relevant requirements. Thus, the available in-situ analytics so far do only allow for limited insights into the reaction mechanism of the FT reaction.

In-situ measurement of the reactant composition under relevant operating conditions offers direct access to several aspects of the actual reaction mechanism and kinetics. Especially for the derivation of reaction and degradation kinetics, spatially-resolved in-situ measurements allow to gain considerably more information than accessible in classical integral reactor setups. Among others, Horn et al. developed a profile reactor technology that was so far applied to basic gas phase reactions [17]. Within this study, it was adapted to the in this regard more challenging multi-phase Fischer-Tropsch synthesis at relevant operating

* Corresponding authors.
E-mail address: florian.wolke@ikts.fraunhofer.de (F. Wolke).

https://doi.org/10.1016/j.catcom.2021.106335
Received 5 March 2021; Received in revised form 9 June 2021; Accepted 26 June 2021
Available online 27 June 2021

conditions, opening the way to a more comprehensive understanding of this reaction. In this very first work, the reaction setup was applied in a study of the influence of reaction temperature, pressure, and promotion on the spatial development of product distribution.

In detail, it is well-known that increasing reaction temperature T leads to an increase in overall reaction rate and conversion level at the expense of average chain length [11]. Additionally, accelerated hydrogenation rate at elevated temperatures leads to increased CH_4 formation [18]. For elevated pressure levels, increasing selectivity towards long-chained hydrocarbons and increased CO conversion is reported [19,20].

Especially for iron-based FT catalysts, promoting elements are applied to affect product selectivity. Among the studied elements, K is often applied due to the resulting increase in chain growth probability and olefin selectivity, however, at the expense of decreased CO conversion [21]. Among the multiple effects of Mo on selectivity of iron-based FT catalysts reported in literature, increased selectivity towards CH_4 and improved long-term stability are the most relevant [22]. Furthermore, improved selectivity towards oxygenates were found for Mo-promoted iron catalysts [23,24].

The chain length distribution of the obtained FT products can be described utilizing the Anderson-Schultz-Flory (ASF) model, according to which the molar fraction x_j of hydrocarbons with a specific carbon number j decreases for higher chain lengths. Molar fraction and carbon number are connected via the so-called chain growth probability α as follows:

$$log x_j = j\ log\ \alpha + log(1-\alpha)\alpha^{-1} \quad (1)$$

For ideal chain growth according to the ASF distribution, α is independent of chain length, yielding a linear correlation. For real FT product mixtures, characteristic deviations from ideal ASF chain length distribution are found, caused by specific aspects concerning reaction mechanism, mass transfer limitations and readsorption [25,26]. Discussed causes for increased selectivity towards CH_4 are an increased probability of termination as well as special active sites for CH_4 formation on the catalyst surface [11]. Since according to the carbide mechanism, the precursor species for products with $j = 2$ exhibits two active sites for monomer addition, probability for propagation to components with $j = 3$ is increased, yielding decreased selectivity towards C_2H_6 and C_2H_4 [27]. This deviation from ideal ASF distribution also highlights that the product distribution of FT presumably cannot be explained by a single mechanism, as a comparable C_2 species does not occur within the CO insertion mechanism.

The aim of this paper is to target first insights into spatially-resolved measurement on iron-based FT synthesis utilizing a compact profile reactor, giving access to experimental data respective the reactant composition in a scalable reactor at relevant operating conditions. Initially, general aspects of the derived reaction profiles of an unpromoted iron-based FT catalyst will be discussed. A specific focus is given to the influence of secondary reactions of alcohols and olefins for unpromoted and promoted iron catalysts.

2. Experimental

2.1. Reactor setup and analytics

In this section, the basic functionalities of the applied *Compact Profile Reactor* (CPR) are described. The actual device was supplied by *Reacnostics* GmbH and entitles a reactor setup, where a tubular fixed-bed reactor (d_i = 4.0 mm) and the enclosed catalyst bed – in case of this study with m_{cat} = 820–850 mg and L_{bed} = 50 mm – are traversed by a capillary, which is equipped with four radially oriented orifices at a specific position. Via these orifices gaseous reaction mixture can be sampled at operating conditions. By moving the fixed-bed reactor including heating unit in spatial direction, the gas phase can be analyzed along the catalyst bed. For this purpose a μ-GC (3-column *Inficon* Fusion; RT-MS 5A, RTQ-Bond, RXI-1MS; TCD) was applied. The maximum scan range of the setup covered L = 60 mm. A flow scheme of the overall experimental setup is given in Fig. 1.

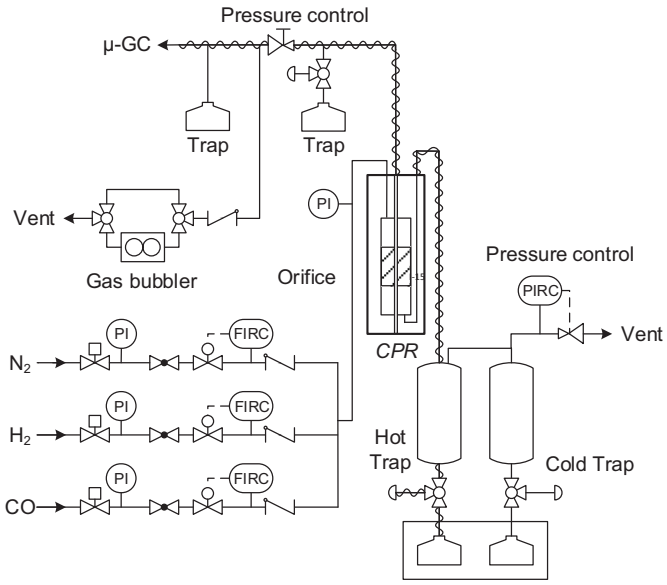

Fig. 1. Flow scheme of the catalytic testing unit applied for CPR experiments.

Feed components were supplied via gas cylinders. Mass flow controllers (*Bronkhorst Hightech BV*) were applied to adjust the actual volumetric flow rates. Downstream of the fixed-bed reactor, the multiphase product flow was separated by using a hot and a cold trap (T_{HT} = 453 K, T_{CT} = 273 K). For analysis of the gaseous components leaving the CPR via the gas probing capillary, respective product mixture was depressurized applying a back pressure regulator. The connecting tubes were heated to T = 453 K. A trap allowed to check for condensed products. The connection to the μ-GC was heated to T = 353 K. A second trap was included to ensure that any possible condensate was removed prior the μ-GC inlet. Besides the measurement of permanent reactant gases H_2 and CO plus internal standard N_2, the μ-GC measurement offered access to C_j paraffin and olefin species ($1 \leq j \leq 9$), while alcohols could be detected for $j \leq 5$. Additionally, the byproduct CO_2 was quantified.

To ensure comparability of the experiments between the CPR and a classical integral reactor with regards to product composition and conversion, reference measurements were performed with a fixed-bed reactor. Details of the applied experimental setup are described elsewhere [28]. The actual reference tubular reactor had an inner diameter of d_i = 15.3 mm, the mass of the catalyst bed was m_{cat} = 6.8 g. On-line analysis of gaseous products was conducted via μ-GC (3-column *Inficon* Fusion; RT-MS 5A, RTQ-Bond, RXI-1MS; TCD), liquid products were analyzed off-line with an *Agilent* 7890B gas chromatograph (HP-1, FID). Reaction conditions for the evaluation experiments were adjusted to the standard operating conditions of the CPR (T = 473 K, p = 2.1 MPa, Ψ = 0.18 ml g_{Fe}^{-1} s^{-1}, H_2/CO = 2/1). While temperature T, pressure p and H_2/CO ratio represent standard values for low temperature Fischer-Tropsch synthesis, the space velocity Ψ was chosen to achieve rather low CO conversion, allowing for the detailed study of the reaction start and, therefore, especially of the influence of secondary reactions on primary products.

2.2. Catalyst preparation

Preparation of the catalysts was conducted via precipitation of aqueous $Fe(NO_3)_3$ solution at T = 343 K, holding pH = 9 with help of aqueous ammonia solution. After stirring, drying, calcination (T = 773 K for t = 10 h) and fractionation (25 μm $\leq d_p \leq$ 100 μm), the obtained

Table 1
Reaction conditions, CO conversion and productivity for the conducted experiments.

Catalyst	Temperature T / K	Pressure p / MPa	Space velocity Ψ / ml g_{Fe}^{-1} s^{-1}	Conversion X_{CO} / -	Paraffin productivity P_{par} / 10^{-7} mol g_{Fe}^{-1} s^{-1}	Olefin productivity P_{ole} / 10^{-7} mol g_{Fe}^{-1} s^{-1}	Alcohol productivity P_{alc} / 10^{-7} mol g_{Fe}^{-1} s^{-1}	CO_2 productivity P_{CO2} / 10^{-7} mol g_{Fe}^{-1} s^{-1}
Fe	473	2.1	0.18	0.06	2.60	1.11	1.06	0.24
Fe	463	2.1	0.18	0.03	1.11	0.41	0.75	0.06
Fe	453	2.1	0.18	0.02	0.58	0.22	0.41	0.03
Fe	473	2.6	0.18	0.06	2.41	0.85	1.07	0.16
$FeK_{0.1}$	473	2.1	0.18	0.02	0.48	0.40	0.15	0.45
$FeCu_{1.0}$	473	2.1	0.18	0.04	2.33	0.73	1.43	0.21
$FeMo_{1.0}$	473	2.1	0.18	0.04	4.12	1.60	1.25	0.77
$FeK_{0.1}Cu_1Mo_1$	473	2.1	0.18	0.04	1.27	0.91	0.51	0.87

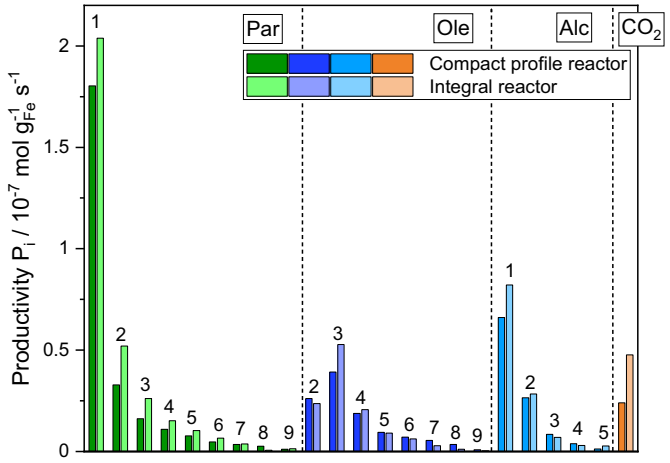

Fig. 2. Comparison of productivity for CPR and reference IR for different product fractions and carbon numbers for an unpromoted Fe catalyst at T = 473 K, p = 2.1 MPa, Ψ = 0.18 ml g_{Fe}^{-1} s^{-1}, H_2/CO = 2.

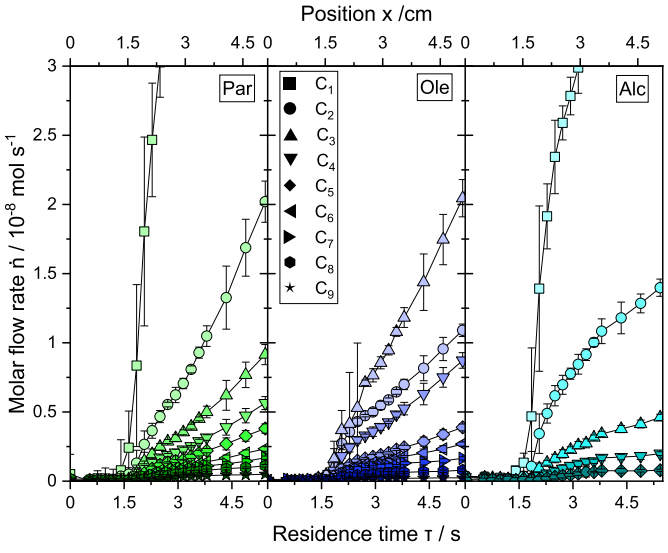

Fig. 3. Development of molar flow rate of individual species of the main product fractions paraffins, olefins, and alcohols over residence time for an unpromoted Fe catalyst at T = 473 K, p = 2.1 MPa, Ψ = 0.18 ml g_{Fe}^{-1} s^{-1}, H_2/CO = 2. On the top x-axis, the corresponding position within the catalyst bed is given.

hematite powder was promoted applying incipient wetness technique. By adding specific volumes of aqueous solutions of KNO_3, Cu $(NO_3)_2$•$3H_2O$ and $(NH_4)_6Mo_7O_{24}$, the amount of promoting elements was adjusted. Calcination of the catalysts was conducted at T = 500 K for t = 10 h. The resulting catalysts are designated as Fe, $FeK_{0.1}$, $FeMo_1$ and $FeK_{0.1}Cu_1Mo_1$. The subscripts represent the mass fraction of the promoter in relation to the amount of reduced iron within the catalyst.

2.3. Catalytic testing

Initial reduction of the oxidized catalysts was performed with hydrogen (T = 673 K, t = 10 h, H_2/N_2= 1/9, p = atm.), followed by an activation period for t > 48 h at reaction conditions (H_2/CO = 2:1, abs. pressure p = 2.1 or 2.6 MPa) to ensure stationary catalytic behavior. The measurement routine for scanning the catalyst bed included five μ-GC analyses per position, resulting in approx. t = 12 h of measurement time for the whole experimental run. As mentioned, a total length of L = 60 mm could be analyzed. The catalyst was fixed in its position by two layers of inert glass wool (L = 5 mm), yielding an actual active bed length of L_{bed} = 50 mm. Movement of the fixed-bed reactor was conducted semi-automatically via an external recipe control. The actual resolution respecting the distance between two positions for gas phase analysis was varied to ensure detailed analysis of regions of interest, especially of the catalyst bed inlet. The axial position within the bed could be converted to a residence time by help of the space velocity Ψ applied in the respective experimental run (Table 1). Over the whole duration of the experiment, the flow of reactant mixture leaving via the capillary was kept constant at approximately 25% of the inlet flow. The local temperature at the actual sampling position was analyzed by using a thermocouple within the capillary. Thermal conductivity of the metal capillary influenced the measured temperature such that pseudo-isothermal conditions were found. However, the results discussed in Section 3 might indicate the occurrence of local temperature maxima. Therefore, the temperature measurements could only be used to determine the average bed temperature.

To address the applicability of the CPR and especially also of the applied analytics, the product compositions at the outlet of the catalyst bed were compared to results from a fixed-bed integral reactor (IR). In Fig. 2 the productivity in dependence of product fraction and chain length is compared for the CPR and the IR setup at similar reaction conditions for an unpromoted Fe catalyst. The comparison is conducted with productivity instead of selectivity, as inaccuracies in gas chromatographical analysis of CO at the achieved low conversions during the experimental runs (Table 1) would also cause inaccuracies in the calculated values for selectivity.

The results in Fig. 2 show that productivity for the individual components is comparable. However, a tendency to a higher productivity for short-chained products and CO_2 for the IR can be deduced. This might be due to the poorer radial heat transfer in the IR. Formation of hot spots leading to increased production of the mentioned compounds is more likely in reactors with higher diameter. However, for the very first assessment of Fischer-Tropsch reaction in such a setup, the resulting agreement allows for the application of the results for a discussion of

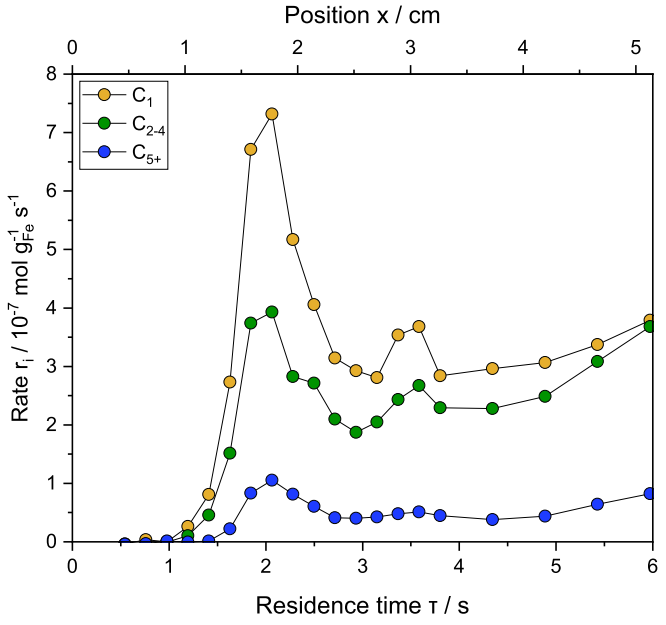

Fig. 4. Local reaction rates for C_1, C_{2-4}, and C_{5+} product formation for an unpromoted Fe catalyst at $T = 473$ K, $p = 2.1$ MPa, $\Psi = 0.18$ ml g_{Fe}^{-1} s^{-1}, $H_2/CO = 2$.

some basic findings.

3. Results and discussion

While characteristic properties of FT catalysts strongly depend on both reaction conditions and applied promoting elements, fundamental attributes can be found commonly. They can be derived from the basic molar flow profiles of the main product fractions of an unpromoted iron-catalyst, which are shown in Fig. 3.

From the reaction profiles for paraffins, olefins and alcohols, the polymerization character of Fischer-Tropsch reaction becomes obvious. Longer hydrocarbons are generated by consecutive addition of monomer units to active chains on the catalyst surface. Consequently, the individual molar flow rate is inversely proportional to carbon number, yielding the characteristic ASF distribution. However, several deviations can be found. For alcohols, decreasing slopes for higher residence times indicate subsequent derivatization. Additionally, the molar flow rate of produced C_2H_4 is lower than for C_3H_6. In contrast, paraffin molar flows indicate chain growth following the ASF model. These effects will be discussed below.

Fig. 4 shows the reaction rate for selected product fractions for the experimental run also shown in Fig. 3. The results show a peak for the formation rates of all product fractions at $\tau = 2$ s. Increased reaction rates at the entrance of the fixed bed are a common observation, which are connected to increased conversion and temperature levels [29]. However, a considerable increase in temperature could not be detected during the measurement, probably also due to the influence of the capillary heat conductivity discussed above. The fact that the reaction not directly starts at the inlet of the catalyst bed ($\tau = 0$ s), but rather for $\tau > 1$ s indicates that sufficient temperature for the reaction to start was not reached at the entrance of the catalyst bed. For the applied setup, the feed gases could only be preheated to $T = 403$ K before entering the reactor. Therefore, the preheating zone consisting of glass wool might have been too short to reach $T = 473$ K at the entrance of the bed. Increasing reaction rates at the outlet of the bed might be due to an underlying temperature profile or due to inaccuracies in measurement.

In Fig. 5, molar flows of the C_1 components CH_4, CH_3OH and CO_2 are plotted over residence time for various reaction temperatures and reaction pressures in order to access the basic catalytic properties of the studied catalyst. As expected, increasing temperatures lead to elevated formation rates for all C_1components.

Once a distinct slope of CH_4 molar flow rate is reached, the respective value remains constant in the covered range of residence time. In contrast to this, the effective rate of CH_3OH formation, especially for elevated temperatures, tends to decrease. This is an evidence for a subsequent derivatization of CH_3OH supported by higher temperatures. It is well-known that elevated temperatures support secondary reactions [21]. This will be discussed in detail later. The WGS rate, which can be derived from CO_2 molar flow rate, accelerates over residence time. This

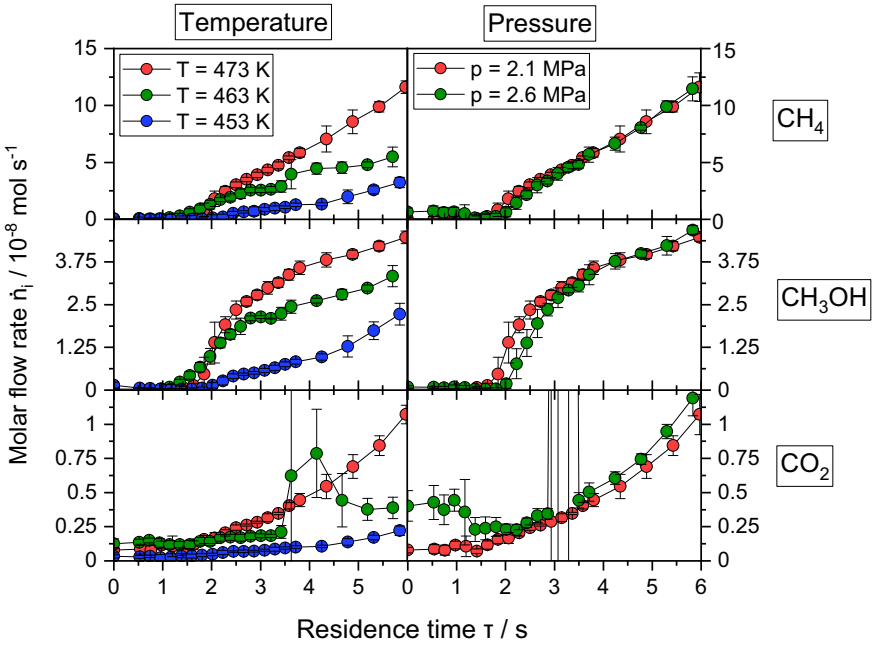

Fig. 5. Influence of reaction temperature and pressure on molar flow profiles of CH_4, CH_3OH and CO_2 for an unpromoted Fe catalyst at $\Psi = 0.18$ ml g_{Fe}^{-1} $s^{-1}$and $H_2/CO = 2$. For the temperature variation, a pressure of $p = 2.1$ MPa was applied, the pressure variation was conducted at $T = 473$ K.

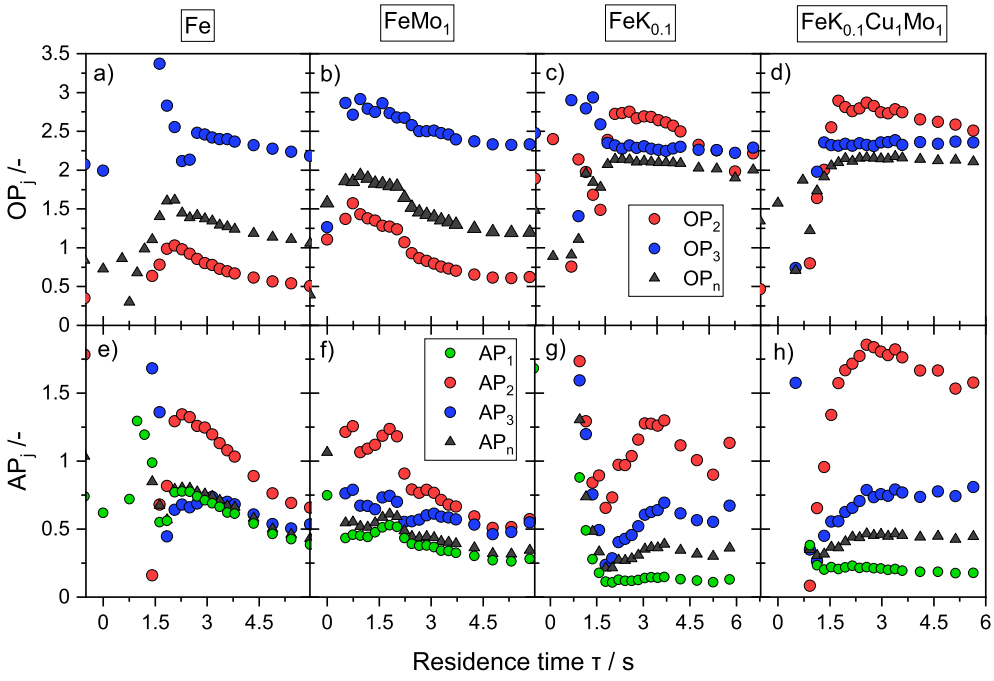

Fig. 6. Olefin-paraffin (OP_j) and alcohol-paraffin (AP_j) ratios over residence time for various Fe catalysts at $T = 473$ K, $p = 2.1$ MPa, $\Psi = 0.18$ ml g_{Fe}^{-1} s^{-1}, $H_2/CO = 2$. For OP_n, methane molar flow was not included in the calculation.

can be explained by increasing WGS activity with increasing conversion for higher residence times, leading to higher water partial pressures. Additionally, the involvement of oxygen-containing intermediates (e.g. formates) in WGS reaction [30] as well as secondary reactions of alcohols [31] might also explain an increased formation of CO_2. It must be noted that the collected data for CO_2 molar flow rates for $3.5\ s < \tau < 4.5\ s$ at $T = 463$ K are subject to measurement errors.

Reviewing the influence of reaction pressure, a negligible impact on the selectivity towards all C_1-components can be stated. As already mentioned, an increase of molar flow rates for CH_4, CH_3OH and CO_2 at increased pressure level, caused by supported coverage of the catalyst surface by both CO and H_2, could be expected. However, for the relatively low pressure difference of $\Delta p = 0.5$ MPa and the small conversion levels (Table 1) might explain the negligible pressure dependency. It must be noted that detected molar flow rates for CO_2 at the entrance of the catalyst bed for $p = 2.6$ MPa are connected to measurement errors due to residual gaseous phase in the probing tube to μ-GC.

The profiles given in Fig. 3 and Fig. 5 already gave an impression of the importance of secondary reactions of alcohols in iron-based FT. Besides alcohols, olefins are also expected to get converted via secondary reactions. Even if alcohols are expected to be more exposed to secondary reactions than olefins [9], a deeper look regarding the influence of these reactions is necessary. For this purpose, the olefin-paraffin ratio

$$OP_j = \frac{\dot{n}_{C_jH_{2j}}}{\dot{n}_{C_jH_{2j+2}}} \tag{2}$$

and the alcohol-paraffin ratio

$$AP_j = \frac{\dot{n}_{C_jH_{2j+1}OH}}{\dot{n}_{C_jH_{2j+2}}} \tag{3}$$

were calculated from the experimental results.

Spatially-resolved measurements provide insights into the dependency of these ratios on residence time, mainly targeting secondary hydrogenation. Fig. 6 shows OP_j and AP_j values over residence time, for various iron-based FT catalysts.

The catalysts considered in Fig. 6 can be divided into two subgroups. For the first subgroup, including the unpromoted Fe and the $FeMo_1$ catalyst, the respective values for OP_j decrease over residence time, indicating secondary hydrogenation of primary olefins to paraffins. The extent of secondary hydrogenation, expressed by constant OP_j values, significantly decreases once K is present as a promoting element, probably due to supported CO coverage of the catalyst surface at the expense of hydrogen adsorption, lowering the hydrogenation activity. Additionally, the reactivity of C_2H_4, as discussed above, seems to be decreased for catalysts promoted with K, which can be deduced comparing the ratios OP_2 and OP_3 to catalysts without K [25]. Assuming stationary conditions for both formation of primary FT products and their conversion into secondary derivates, an intermediate maximum of the productivity of primary FT product with a subsequent decrease of the respective species as well as an increase in secondary products can be expected. Consequently, the molar flow ratio of primary and secondary species, e.g. OP_j, would decrease over residence time. This trend can be identified for the catalysts without K promotion, indicating the described olefin hydrogenation to paraffins. Reviewing the AP_j ratio to evaluate the extent of secondary conversion of primary alcohols to the respective paraffin analogues, a similar trend becomes apparent. While AP_j values for unpromoted Fe and $FeMo_1$ catalyst decrease over residence time, the ratio remains constant for K-promoted catalysts. Assuming stationary conditions with consecutive parallel formation of paraffins and alcohols, the AP_j ratio is expected to remain constant in the absence of secondary reactions. In contrast to OP_j, a distinct chain length dependency of AP_j can be found, which can be attributed to the difference in chain growth probabilities between alcohols and paraffins, leading to lower AP_j with increasing chain length. In detail, $\alpha_{Par} = 0.57$ is comparable to $\alpha_{Ole} = 0.56$, while $\alpha_{Alc} = 0.39$.

Besides hydrogenation, dehydrogenation to aldehydes as well as dehydration to olefins might be additional reaction pathways [31]. Dehydrogenation would also lead to a decrease in AP_j ratio. As with the current analytics, no information on aldehyde or ketone formation could be derived, the extent of this secondary reaction cannot be estimated. This would be a topic for studies with an updated setup. The dehydration of primary alcohols to olefins would lead to an increase in OP_j ratio. This cannot be derived from the results shown in Fig. 6. The decreasing or

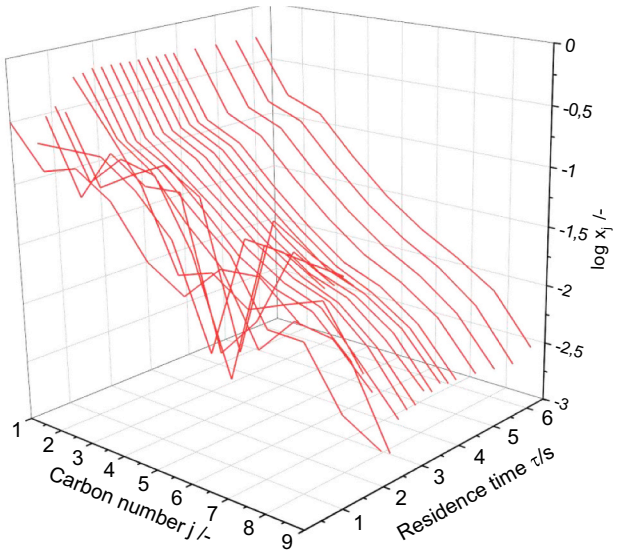

Fig. 7. Development of ASF distribution for an unpromoted Fe catalyst at $T = 473$ K, $p = 2.1$ MPa, $\Psi = 0.18$ ml g_{Fe}^{-1} s^{-1}, $H_2/CO = 2$.

constant OP_j ratios lead to the conclusion that the extent of dehydration of primary alcohols is negligible, which is in line with literature [31].

It must be mentioned that values for OP_j and AP_j given for short residence times of $\tau < 2$ s are subject to larger scatter due to the very low product concentrations at the inlet of the bed that causes a higher uncertainty of the μ-GC measurement.

The discussion of Fig. 6 allowed for the assessment of the extent of secondary reactions of olefins and alcohols, but not of their influence on chain growth distribution. In Fig. 7 the ASF distribution $\log(x_j)$ is plotted as a function of time. For residence times $\tau < 2$ s, the conversion respecting CO is on a small level, associated with small molar product flow rates causing higher uncertainties in the analysis, as discussed above. Therefore, the plotted ASF distribution for the inlet of the bed show a considerable scatter. However, for $\tau > 2$ s, ASF distribution remains constant, indicating a steady state of consecutive chain growth to FT products. For residence times $\tau > 2$ s, where α can be calculated with sufficient certainty, the calculated value of $\alpha = 0.55$ remains constant. Thus, the influence of secondary reactions leading to reinitiation of chain growth, e.g. caused by readsorption of short-chained olefins [27] or alcohols [9] is not pronounced enough to effect the chain length distribution for the studied conditions and for the applied catalyst.

4. Conclusions

Within this study, a compact profile reactor was applied to measure spatially-resolved reaction profiles for an iron-based Fischer-Tropsch catalyst. Initially, comparability of obtained experimental data to a common fixed-bed integral reactor at similar reaction conditions was proven. The derived molar flow rates of FT reaction products, respective reaction rates, olefin-to-paraffin, and alcohol-to-paraffin ratios as well as chain growth probabilities could be monitored in dependence of residence time. The influence of secondary conversion of primary formed olefins and alcohols into derivatives as paraffins was shown and could be monitored over residence time. An overall trend of suppressed secondary conversion of primary olefins and alcohols to paraffins could be shown for iron catalysts promoted with K, since both olefin-paraffin and alcohol-paraffin ratios remained constant throughout the catalyst bed. However, an influence of reinitiation of chain growth via readsorbed olefins or alcohols on ASF distribution could not be found.

Based on these fundamental analyses, further experiments must be conducted to gain deeper insights into the complex reaction mechanism of Fischer-Tropsch reaction. The demonstrated experimental approach offers high potential in this regard.

Credit author statement

Florian Wolke: Conceptualization, Investigation, Methodology, Writing original draft - Review & Editing

Yiwen Hu: Writing, Conceptualization, Methodology, Review & Editing

Michael Schmidt: Conceptualization, Review & Editing

Oliver Korup: Conceptualization, Review & Editing

Raimund Horn: Conceptualization, Supervision, Review & Editing

Erik Reichelt: Funding, Supervision, Conceptualization, Methodology, Writing, Review & Editing

Matthias Jahn: Funding, Supervision, Resources, Review & Editing

Alexander Michaelis: Funding, Supervision, Resources, Review & Editing

Declaration of Competing Interest

The authors declare that they have no known competing financial interests or personal relationships that could have appeared to influence the work reported in this paper.

Acknowledgment

This research was supported by the German Federal Ministry for Economic Affairs and Energy (03EIV031B).

References

[1] G. Herz, E. Reichelt, M. Jahn, Techno-economic analysis of a co-electrolysis-based synthesis process for the production of hydrocarbons, Appl. Energy 215 (2018) 309–320.
[2] H.T. Luk, C. Mondelli, D.C. Ferré, J.A. Stewart, J. Pérez-Ramírez, Status and prospects in higher alcohols synthesis from syngas, Chem. Soc. Rev. 46 (2017) 1358–1426.
[3] D.H. Chun, G.B. Rhim, M.H. Youn, D. Deviana, J.E. Lee, J.C. Park, H. Jeong, Brief review of precipitated Iron-based catalysts for low-temperature Fischer–Tropsch synthesis, Top. Catal. 63 (2020) 793–809.
[4] B. Todic, L. Nowicki, N. Nikacevic, D.B. Bukur, Fischer–Tropsch synthesis product selectivity over an industrial iron-based catalyst: effect of process conditions, Catal. Today 261 (2016) 28–39.
[5] E. de Smit, B.M. Weckhuysen, The renaissance of iron-based Fischer-Tropsch synthesis: on the multifaceted catalyst deactivation behaviour, Chem. Soc. Rev. 37 (2008) 2758–2781.
[6] W. Ma, G. Jacobs, D.E. Sparks, J.L. Klettlinger, C.H. Yen, B.H. Davis, Fischer–Tropsch synthesis and water gas shift kinetics for a precipitated iron catalyst, Catal. Today 275 (2016) 49–58.
[7] T.J. Okeson, K. Keyvanloo, J.S. Lawson, M.D. Argyle, W.C. Hecker, On the kinetics and mechanism of Fischer–Tropsch synthesis on a highly active iron catalyst supported on silica-stabilized alumina, Catal. Today 261 (2016) 67–74.
[8] J. Schweicher, A. Bundhoo, N. Kruse, Hydrocarbon chain lengthening in catalytic CO hydrogenation: evidence for a CO-insertion mechanism, J. Am. Chem. Soc. 134 (2012) 16135–16138, https://doi.org/10.1021/ja3068484.
[9] B.H. Davis, Fischer–Tropsch synthesis: reaction mechanisms for iron catalysts, Catal. Today 141 (2009) 25–33.
[10] M.E. Dry, The Fischer-Tropsch process: 1950-2000, Catal. Today (2002) 227–241.
[11] G.P. van der Laan, A.A.C.M. Beenackers, Kinetics and selectivity of the Fischer–Tropsch synthesis: a literature review, Catal. Rev. 41 (1999) 255–318.
[12] N. Fischer, M. Claeys, In situ characterization of Fischer–Tropsch catalysts: a review, J. Phys. D. Appl. Phys. 53 (2020) 293001.
[13] M.R. Nielsen, A.B. Moss, A.S. Bjørnlund, X. Liu, A. Knop-Gericke, A.Y. Klyushin, J.-D. Grunwaldt, T.L. Sheppard, D.E. Doronkin, A. Zimina, T.E.L. Smitshuysen, C. D. Damsgaard, J.B. Wagner, T.W. Hansen, Reduction and carburization of iron oxides for Fischer–Tropsch synthesis, J. Energy Chem. 51 (2020) 48–61.
[14] Q. Chang, C. Zhang, C. Liu, Y. Wei, A.V. Cheruvathur, A.I. Dugulan, J. W. Niemantsverdriet, X. Liu, Y. He, M. Qing, L. Zheng, Y. Yun, Y. Yang, Y. Li, Relationship between Iron carbide phases (ε-Fe_2C, Fe $_7C_3$ and χ-Fe_5C_2) and catalytic performances of Fe/SiO_2 Fischer–Tropsch catalysts, ACS Catal. 8 (2018) 3304–3316.
[15] E. de Smit, A.M. Beale, S. Nikitenko, B.M. Weckhuysen, Local and long range order in promoted iron-based Fischer–Tropsch catalysts: a combined in situ X-ray absorption spectroscopy/wide angle X-ray scattering study, J. Catal. 262 (2009) 244–256.
[16] S. Janbroers, P.A. Crozier, H.W. Zandbergen, P.J. Kooyman, A model study on the carburization process of iron-based Fischer–Tropsch catalysts using in situ TEM–EELS, Appl. Catal. B Environ. 102 (2011) 521–527.

[17] O. Korup, S. Mavlyankariev, M. Geske, C.F. Goldsmith, R. Horn, Measurement and analysis of spatial reactor profiles in high temperature catalysis research, Chem. Eng. Process. Process Intensif. 50 (2011) 998–1009.
[18] M.E. Dry, The Fischer-Tropsch synthesis, Catal. Sci. Tech. (1981) 159–255.
[19] F.G. Botes, J.W. Niemantsverdriet, J. van de Loosdrecht, A comparison of cobalt and iron based slurry phase Fischer–Tropsch synthesis, Catal. Today 215 (2013) 112–120.
[20] M. Pijolat, V. Perrichon, Synthesis of alcohols from CO and H_2 on a Fe-Al_2O_3 catalyst at 8-30 bars pressure, Appl. Catal. (1985) 321–333.
[21] D.B. Bukur, D. Mukesh, S.A. Patel, Promoter effects on precipitated iron catalysts for Fischer-Tropsch synthesis, Ind. Eng. Chem. Res. 29 (1990) 194–204.
[22] W. Ma, E.L. Kugler, J. Wright, D.B. Dadyburjor, Mo−Fe catalysts supported on activated carbon for synthesis of liquid fuels by the Fischer−Tropsch process: effect of Mo addition on reducibility, activity, and hydrocarbon selectivity, Energy Fuel 20 (2006) 2299–2307.
[23] A. Alayat, E. Echeverria, D.N. Mcllroy, A.G. McDonald, Enhancement of the catalytic performance of silica nanosprings (NS)-supported iron catalyst with copper, molybdenum, cobalt and ruthenium promoters for Fischer-Tropsch synthesis, Fuel Process. Technol. 177 (2018) 89–100.
[24] X. Cui, J. Xu, C. Zhang, Y. Yang, P. Gao, B. Wu, Y. Li, Effect of pretreatment on precipitated Fe–Mo Fischer–Tropsch catalysts: morphology, carburization, and catalytic performance, J. Catal. 282 (2011) 35–46.
[25] D. Förtsch, K. Pabst, E. Groß-Hardt, The product distribution in Fischer–Tropsch synthesis: an extension of the ASF model to describe common deviations, Chem. Eng. Sci. 138 (2015) 333–346.
[26] J.H. Yang, H.-J. Kim, D.H. Chun, H.-T. Lee, J.-C. Hong, H. Jung, J.-I. Yang, Mass transfer limitations on fixed-bed reactor for Fischer–Tropsch synthesis, Fuel Process. Technol. 91 (2010) 285–289.
[27] R. Snel, R.L. Espinoza, Secondary reactions of primary products of the Fischer-Tropsch synthesis part 1: the role of ethene, J. Mol. Catal. (1987) 237–247.
[28] M. Schaller, E. Reichelt, M. Jahn, Iron-based Fischer-Tropsch catalysts for higher alcohol synthesis, Chemie Ingenieur Technik 90 (2018) 713–720.
[29] P. Kaiser, A. Jess, Modeling of multitubular reactors for Iron- and cobalt-catalyzed Fischer-Tropsch syntheses for application in a power-to-liquid process, Energy Technol. 2 (2014) 486–497.
[30] D.B. Bukur, B. Todic, N. Elbashir, Role of water-gas-shift reaction in Fischer–Tropsch synthesis on iron catalysts: a review, Catal. Today 275 (2016) 66–75.
[31] Y. Wang, B.H. Davis, Fischer-Tropsch synthesis. Conversion of alcohols over iron oxide and iron carbide catalysts, Appl. Catalysis A: General (1999) 277–285.